Inorg. Chem. **2003**, *42*, 1045–1056

Dinuclear Cyano Complexes of Cobalt(III) and Iron(III) Containing Noninnocent 1,2,4,5-Tetrakis(2-pyridinecarboxamido)benzene Bridging Ligands

Udo Beckmann, Eckhard Bill, Thomas Weyhermüller, and Karl Wieghardt*

Max-Planck-Institut für Strahlenchemie, Stiftstrasse 34-36, D-45470 Mülheim an der Ruhr, Germany

Received August 16, 2002

Two new dinucleating ligands 1,2,4,5-tetrakis(2-pyridinecarboxamido)benzene, H_4(tpb), and 1,2,4,5-tetrakis(4-*tert*-butyl-2-pyridinecarboxamido)benzene, H_4(tbpb), have been synthesized, and the following dinuclear cyano complexes of cobalt(III) and iron(III) have been isolated: $Na_2[Co^{III}_2(tpb)(CN)_4]$ (**1**); $[N(n\text{-}Bu)_4]_2[Co^{III}_2(tbpb)(CN)_4]$ (**2**); $[Co^{III}_2(tbpb^{ox2})(CN)_4]$ (**3**); $[N(n\text{-}Bu)_4]_2[Fe^{III}_2(tpb)(N_3)_4]$ (**4**); $[N(n\text{-}Bu)_4]_2[Fe^{III}_2(tpb)(CN)_4]$ (**5**); $[N(n\text{-}Bu)_4]_2[Fe^{III}_2(tbpb)(CN)_4]$ (**6**). Complexes **2**–**4** and **6** have been structurally characterized by X-ray crystallography at 100 K. From electrochemical and spectroscopic (UV–vis, IR, EPR, Mössbauer) and magnetochemical investigations it is established that the coordinated central 1,2,4,5-tetraamidobenzene entity in the cyano complexes can be oxidized in two successive one-electron steps yielding paramagnetic $(tbpb^{ox1})^{3-}$ and diamagnetic $(tbpb^{ox2})^{2-}$ anions. Thus, complex **6** exists in five characterized oxidation levels: $[Fe^{III}_2(tbpb^{ox2})(CN)_4]^0$ ($S = 0$); $[Fe^{III}_2(tbpb^{ox1})(CN)_4]^-$ ($S = {}^1/_2$); $[Fe^{III}_2(tbpb)(CN)_4]^{2-}$ ($S = 0$); $[Fe^{III}Fe^{II}(tbpb)(CN)_4]^{3-}$ ($S = {}^1/_2$); $[Fe^{II}_2(tbpb)(CN)_4]^{4-}$ ($S = 0$). The iron(II) and (III) ions are always low-spin configurated. The electronic structure of the paramagnetic iron(III) ions and the exchange interaction of the three-spin system $[Fe^{III}_2(tbpb^{ox1})(CN)_4]^-$ are characterized in detail. Similarly, for **2** three oxidation levels have been identified and fully characterized: $[Co^{III}_2(tbpb)(CN)_4]^{2-}$ ($S = 0$); $[Co^{III}_2(tbpb^{ox1})(CN)_4]^-$ ($S = {}^1/_2$); $[Co^{III}_2(tbpb^{ox2})(CN)_4]^0$. The crystal structures of **2** and **3** clearly show that the two electron oxidation of **2** yielding **3** affects only the central tetraamidobenzene part of the ligand.

Introduction

Recently, we[1] and others[2,3] have discovered that 1,2-bis(pyridine-2-carboxamido)benzenate(2−) coordinated to iron(III) is a noninnocent ligand[1,2] in the sense that it can be oxidized to its paramagnetic π radical monoanion and, finally, to its diamagnetic neutral benzoquinone form. The chemistry and magnetochemistry of such coordinated organic π-radicals is currently under intense investigation because interesting magnetic materials may be anticipated.[4−7] Here we synthesized binucleating ligands of the type 1,2,4,5-tetrakis(2-pyridinecarboxamido)benzene, namely H_4(tpb) and H_4(tbpb) shown in Chart 1, which can bind two paramagnetic metal ions such as for example iron(III). It was hoped that the ligand is again noninnocent and that the π−radical oxidation level is accessible to assemble magnetic molecular systems consisting of two paramagnetic metal ions bridged by an organic π radical.

Previously, two similar studies have appeared in the literature. Collins et al.[8] have used the binucleating ligand 1,2,4,5-tetrakis(2-hydroxy-2-methylpropanamido)benzene, and Aukauloo and Journaux et al.[9] have synthesized *N*,*N*′,*N*″,*N*‴-1,2,4,5-benzenetetrayltetrakis(oxamate). Vanadium and co-

* To whom correspondence should be addressed. E-mail: wieghardt@mpi-muelheim.mpg.de.

(1) Dutta, S. K.; Beckmann, U.; Bill, E.; Weyhermüller, T.; Wieghardt, K. *Inorg. Chem.* **2000**, *39*, 3355.
(2) Patra, A. K.; Ray, M.; Mukherjee, R. *Inorg. Chem.* **2000**, *39*, 652.
(3) Mak, S.-T.; Wong, W.-T.; Yam, V. W.-W.; Lai, T.-F.; Che, C.-M. *J. Chem. Soc., Dalton Trans.* **1991**, 1915.
(4) Sono, M.; Roach, M. P.; Coulter, E. D.; Dawson, J. H. *Chem. Rev.* **1996**, *96*, 2841.
(5) Miller, J. S.; Epstein, A. J. *Chem. Commun.* **1998**, 1319.
(6) Iwamura, H.; Inove, K.; Koga, N. *New J. Chem.* **1998**, 201.
(7) Caneschi, A.; Gatteschi, D.; Rey, P. *Prog. Inorg. Chem.* **1991**, *39*, 331.
(8) Gordon-Wylie, S. W.; Claus, B. L.; Horwitz, C. P.; Leychis, Y.; Workman, J. M.; Marzec, A. J.; Clark, G. R.; Rickard, C. E. F.; Couklin, B. J.; Sellers, S.; Yee, G. T.; Collins, T. J. *Chem.—Eur. J.* **1998**, *4*, 2173.
(9) Aukauloo, A.; Ottenwaelder, X.; Ruiz, R.; Poussereau, S.; Pei, Y.; Journaux, Y.; Fleurat, P.; Volatron, F.; Cervera, B.; Munoz, M. C. *Eur. J. Inorg. Chem.* **1999**, 1067.

10.1021/ic020518z CCC: $25.00
Published on Web 01/24/2003

Chart 1. Ligands and Complexes

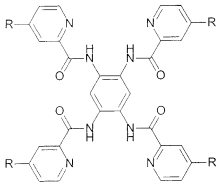

R = H H_4(tpb)
R = tert-butyl H_4(tbpb)

$Na_2[Co^{III}_2(tpb)(CN)_4]$ (1)

$[N(n\text{-}Bu)_4]_2[Co^{III}_2(tbpb)(CN)_4]$ (2)

$[Co^{III}_2(tbpb^{ox2})(CN)_4]$ (3)

$[N(n\text{-}Bu)_4]_2[Fe^{III}_2(tpb)(N_3)_4]$ (4)

$[N(n\text{-}Bu)_4]_2[Fe^{III}_2(tpb)(CN)_4]$ (5)

$[N(n\text{-}Bu)_4]_2[Fe^{III}_2(tbpb)(CN)_4]$ (6)

balt complexes have been synthesized with the former, and a dinuclear nickel(II) species has been synthesized with the latter ligand.

Experimental Section

Synthesis of Ligands and Complexes. 1,2,4,5-Tetrakis(2-pyridinecarboxamido)benzene, H_4(tpb). To a solution of 1,2,4,5-tetraaminobenzene tetrahydrochloride (1.1 g; 4 mmol) in pyridine (5 mL) was added a solution of picolinic acid (2.0 g; 16 mmol) in pyridine (5 mL). Triphenyl phosphite (5.0 g; 16 mmol) was then added to the reaction mixture, which was heated to 100 °C for 5 h. After storage of the resulting solution at 4 °C for 48 h the precipitate formed was filtered off, washed with water (10 mL) and cold ethanol. A yellow powder (1.7 g; 76%) was obtained. Mp (uncorrected): 354 °C. Anal. Calcd for $C_{30}H_{22}N_8O_4$: C, 64.51; H, 3.97; N, 20.06. Found: C, 64.3; H, 4.0; N, 20.2. EI mass spectrum (*m*/*z*): 558, $\{M^+\}$. The ligand is insoluble in all common solvents.

1,2,4,5-Tetrakis(4-*tert*-butyl-2-pyridinecarboxamido)benzene, H_4(tbpb). To a solution of 1,2,4,5-tetraaminobenzene tetrahydrochloride (1.1 g; 4 mmol) in pyridine (10 mL) was added 4-*tert*-butylpicolinic acid hydrochloride (3.5 g; 16 mmol) with stirring. To this reaction mixture was added dropwise triphenyl phosphite (5.0 g; 16 mmol). After heating of the mixture to 100 °C for 12 h and cooling to 20 °C, the pyridine solvent was removed by evaporation under reduced pressure. The brown-red tenacious residue was dissolved in ethanol (30 mL) with heating to reflux for 15 min. The solution was allowed to stand at 4 °C for 48 h, after which time a yellow precipitate was filtered off: yield 0.91 g (30%); mp (uncorrected) 321 °C. Anal. Calcd for $C_{46}H_{54}N_8O_4$: C, 70.56; H, 6.95; N, 14.31. Found: C, 69.96; H, 7.1; N, 14.2. ^{1}H NMR (400 MHz, CD_2Cl_2; δ): 1.38 (36H, s, *tert*-butyl); 7.49 (4H, m, aromatic); 8.34 (4H, s, arom); 8.44 (2H, m, arom); 8.48 (4H, m, arom); 10.29 (4H, s, NH). ^{13}C NMR (100.6 MHz, CD_2Cl_2; δ): 30.6; 35.4; 120.0, 120.6, 124.0, 128.5, 129.5, 148.6, 150.0, 162.6, 163.7. EI mass spectrum (*m*/*z*): 783, $\{M^+\}$.

$Na_2[Co^{III}_2(tpb)(CN)_4]\cdot H_2O$ (1·H_2O). To a boiling solution of H_4(tpb) (0.56 g; 1.0 mmol) in methanol (100 mL) was added a solution of 0.6 M $[N(n\text{-}Bu)_4](OCH_3)$ in methanol (6.7 mL; 4.0 mmol). $CoCl_2\cdot 6H_2O$ (0.48 g; 2.0 mmol) dissolved in 2 mL of methanol was then added. The brown reaction mixture was heated to reflux in the presence of air for 2 h after which time NaCN (0.20 g; 4.0 mmol) was added with stirring. From the brown-red solution a microcrystalline precipitate of **1** formed within minutes. Yield: 0.5 g (40%). Anal. Calcd for $C_{34}H_{20}N_{12}O_5Co_2Na_2$: C, 48.59; H, 2.40; N, 20.00; Co, 14.02; Na, 5.47. Found: C, 48.4; H, 2.2; N, 20.2; Co, 13.8; Na, 5.6. ^{1}H NMR (400 MHz, D_2O; δ): 7.84 (4H, ddd, ^3J = 7.3, ^3J = 5.8, ^4J = 1.4 Hz); 8.07 (4H, dd, ^3J = 7.8 Hz); 8.28 (4H, dd, ^3J = 7.7, ^3J = 7.7 Hz); 9.14 (4H, d, ^3J = 5.5 Hz); 9.94 (2H, s). ESI (neg ion) mass spectrum (*m*/*z*): 1018.5, $\{[N(n\text{-}Bu)_4][Co_2(tpb)(CN)_4]\}^-$; 750.0, $\{M^{2-} - 1CN\}^-$. When $[N(n\text{-}Bu)_4]$-CN was used in the above procedure, the salt $[N(n\text{-}Bu)_4][Co^{III}2$-$(tpb)(CN)_4]$ was obtained in 50% yield.

$[N(n\text{-}Bu)_4]_2[Co^{III}_2(tbpb)(CN)_4]\cdot 3CH_3OH\cdot H_2O$ (2·3CH_3OH·H_2O). To a solution of the ligand H_4(tbpb) (0.39 g; 0.5 mmol) in methanol (30 mL) was added a 20% methanolic solution of $[N(n\text{-}Bu)_4]OCH_3$ (3.4 mL, 2 mmol). A solution of $CoCl_2\cdot 6H_2O$ (0.24 g; 1.0 mmol) in CH_3OH (5 mL) and then a methanolic (5 mL) solution of $[N(n\text{-}Bu)_4]CN$ (0.54 g; 2.0 mmol) were added with stirring. The resulting deep red solution was heated to reflux for 1 h. The volume of the cooled and filtered solution was reduced by half by rotary evaporation. After storage of the solution at 4 °C for 12 h a deep red crystalline product of **2** was obtained. Yield: 0.62 g (77%). Single crystals of **2** were grown from a methanolic solution of **2** by slow diethyl ether diffusion. Anal. Calcd for $C_{85}H_{136}N_{14}O_8Co_2$: C, 63.81; H, 8.57; N, 12.26; Co, 7.37. Found: C, 63.6; H, 8.4; N, 12.1; Co, 7.3. ^{1}H NMR (500 MHz, CD_2Cl_2; δ): 0.75 (24H, t, CH_3); 1.17 (16 H, m, CH_2); 1.45 (12H, m, CH_2); 1.45 (36H, s, *tert*-butyl); 2.85 (12H, m, CH_2), 7.60 (4H, dd); 8.11 (4H, d); 8.82 (4H, dd); 10.09 (2H, s). ESI (neg ion) mass spectrum (*m*/*z*): 1242.5, $\{M^{2-} + [N(n\text{-}Bu)_4]^+\}^-$; 974.2, $\{M^{2-} - CN\}^-$.

$[Co^{III}_2(tbpb^{ox2})(CN)_4]\cdot 4CD_2Cl_2$ (3·4CD_2Cl_2). Controlled potential electrolysis at 1.0 V vs Fc^+/Fc under an Ar blanketing atmosphere at −25 °C of a solution of CD_2Cl_2 (10 mL) containing 30 mg of complex **2** and $[N(n\text{-}Bu)_4]PF_6$ (0.39 g) as supporting electrolyte (removal of 2 electrons/dianion of **2**) yields a deep green solution the volume of which was reduced by half by passing an Ar stream through the oxidized solution. Upon standing at 10 °C for 12 h red crystals of **3** and solid colorless $[N(n\text{-}Bu)_4]PF_6$ precipitated. The crystals were separated manually under a microscope. Yield: 23 mg (86%). ^{1}H NMR (400 MHz, CD_2Cl_2; δ): 7.99 (4H, dd); 8.36 (4H, d); 8.99 (4H, dd); 9.92 (2H, s). Aromatic proton signals of **3** are given only.

$[N(n\text{-}Bu)_4]_2[Fe^{III}_2(tpb)(N_3)_4]\cdot 3CH_3CN$ (4·3CH_3CN). To a solution of the ligand H_4(tpb) (0.28 g; 0.5 mmol) in methanol (40 mL) was added 2 mL of a 1.0 M methanolic solution of NaOH. A solution of $FeCl_3\cdot 6H_2O$ (0.27 g; 1.0 mmol) in CH_3OH (5 mL) was added. The resulting solution was heated to reflux for 6 h. The resulting brown precipitate was filtered off and suspended in acetone (40 mL) to which NaN_3 (1.3 g; 20 mmol) and $[N(n\text{-}Bu)_4]Cl$ (0.28 g; 1.0 mmol) were then added. After being heated to reflux for 5 h, the cooled solution was filtered (excess NaN_3 was discarded) and the acetone solvent was removed by evaporation under reduced pressure. To the residual tenacious brown oil was added acetonitrile (5 mL). After addition of toluene (40 mL), the resulting clear, brown solution was allowed to stand in the refrigerator for 2−3 days. Small, brown-black crystals of **4** precipitated. Yield: 0.11 g (15%). Anal. Calcd for $C_{68}H_{99}N_{25}O_4Fe_2$: C, 56.62; H, 6.92; N, 24.28; Fe, 7.74. Found: C, 56.4; H, 7.1; N, 24.1; Fe, 8.0.

$[N(n\text{-}Bu)_4]_2[Fe^{III}_2(tpb)(CN)_4]$ (5). To a solution of the ligand H_4(tpb) (0.28 g; 0.5 mmol) in methanol (40 mL) was added 2 mL of a 1.0 M methanolic solution of NaOH. A solution of $FeCl_3\cdot 6H_2O$ (0.27 g; 1.0 mmol) dissolved in CH_3OH (5 mL) and a solution of $[N(n\text{-}Bu)_4](CN)$ (0.54 g; 2.0 mmol) in CH_3OH (5 mL) were added. The resulting mixture was heated to reflux for 6 h. After filtration and cooling brown black microcrystals of **5** precipitated at 4 °C within 12 h. Yield: 0.27 g (43%). Anal. Calcd for $C_{66}H_{90}N_{14}O_4Fe_2$: C, 63.15; H, 7.23; N, 15.62; Fe, 8.90. Found:

Table 1. Crystallographic Data for **2**·2.8MeOH·1.2H_2O, **3**·4CD_2Cl_2, **4**·3CH_3CN, and **6**·3.5MeOH·0.5Et_2O

	2·2.8MeOH·1.2H_2O	**3**·4CD_2Cl_2	**4**·3CH_3CN	**6**·3.5MeOH·0.5Et_2O
chem formula	$C_{84.8}H_{135.6}Co_2N_{14}O_8$	$C_{54}H_{50}D_8Co_2N_{12}O_4Cl_8$	$C_{68}H_{99}Fe_2N_{25}O_4$	$C_{87.5}H_{141}Fe_2N_{14}O_8$
fw	1597.13	1340.58	1442.42	1628.84
space group	$P2_1/c$, No. 14	$P\bar{1}$, No. 2	$P2_1/c$, No. 14	$P2_1/c$, No. 14
a, Å	13.9684(12)	10.3351(8)	14.5944(12)	14.0065(12)
b, Å	27.061(2)	13.1244(10)	20.215(2)	27.069(2)
c, Å	12.8132(12)	13.3233(11)	14.4511(12)	12.7579(10)
α, deg	90	113.72(2)	90	90
β, deg	95.76(2)	103.35(2)	111.34(2)	95.38(2)
γ, deg	90	102.22(2)	90	90
V, Å	4818.9(7)	1512.8(12)	3971.1(3)	4815.7(7)
Z	2	1	2	2
T, K	100(2)	100(2)	100(2)	100(2)
ρ_{calcd}, g cm^{-3}	1.101	1.471	1.206	1.123
diffractometer used	Siemens SMART	Siemens SMART	Nonius Kappa-CCD	Siemens SMART
reflcns collcd/ θ_{max}	41 869/55.00	16 013/66.28	61 805/54.98	39 184/52.00
unique reflcns/$I > 2\sigma(I)$	10 874/7362	9718/6003	9071/6302	9373/6197
no. of params/restraints	503/1	371/0	445/4	526/30
μ(Mo Kα), cm^{-1}	3.99	9.56	4.25	3.58
R1[a]/goodness of fit[b]	0.0664/1.033	0.0519/0.909	0.0719/1.064	0.0606/1.025
wR2[c] ($I > 2\sigma(I)$)	0.1773	0.1092	0.2236	0.1449

[a] Observation criterion: $I > 2\sigma(I)$. R1 = $\Sigma||F_o| - |F_c||/\Sigma|F_o|$. [b] GooF = $[\Sigma[w(F_o^2 - F_c^2)^2]/(n-p)]^{1/2}$. [c] wR2 = $[\Sigma[w(F_o^2 - F_c^2)^2]/\Sigma[w(F_o^2)^2]]^{1/2}$, where $w = 1/\sigma^2(F_o^2) + (aP)^2 + bP$ and $P = (F_o^2 + 2F_c^2)/3$.

C, 63.2; H, 7.1; N, 15.4; Fe, 8.7. ESI (neg ion) mass spectrum (*m*/*z*): 744.1, $\{M^{2-} - 1CN\}^-$.

[N(*n*-Bu)$_4$]$_2$[Fe$^{III}_2$(tbpb)(CN)$_4$]·3.5CH_3OH·0.5(C_2H_5)$_2$O (6·3.5CH_3OH·0.5(C_2H_5)$_2$O). To a suspension of the ligand H_4(tbpb) (0.20 g; 0.25 mmol) in CH_3OH (20 mL) was added 1.7 mL of a 1.0 M methanolic solution of [N(*n*-Bu)$_4$](OCH_3) (20%) and $FeCl_3$·6H_2O (0.135 g; 0.50 mmol) dissolved in 5 mL of CH_3OH. Finally, [N(*n*-Bu)$_4$](CN) (0.27 g; 1.0 mmol) dissolved in 5 mL of CH_3OH was added. The mixture was heated to reflux for 3−4 h. The resulting cooled deep brown solution was filtered, and half of the solvent was removed by rotary evaporation. After the mixture was standing at 4 °C for 12 h, brown black microcrystalline **6** was obtained. Yield: 0.14 g (38%). From a concentrated methanol solution of **6** single crystals were slowly grown by diffusion of diethyl ether: [N(*n*-Bu)$_4$][Fe$^{III}_2$(tbpb)(CN)$_4$]·3.5CH_3OH·0.5Et_2O. Anal. Calcd for $C_{82}H_{122}N_{14}O_4Fe_2$: C, 66.56; H, 8.31; N, 13.25; Fe, 7.55. Found: C, 66.4; H, 8.4; N, 12.9; Fe, 7.5. ESI (neg ion) natural isotopic ratio (*m*/*z*): 1237.6, 968.2, 942, and 970.3 for a 100% ^{57}Fe-enriched sample.

X-ray Crystallographic Data Collection and Refinement of the Structures. Dark red-violet single crystals of **2**−**4** and an orange-red crystal of **6** were coated with perfluoropolyether. Suitable crystals were picked up with a glass fiber and were immediately mounted in the nitrogen cold stream of the diffractometers to prevent loss of solvent. Intensity data were collected at 100 K using graphite-monochromated Mo Kα radiation (λ = 0.710 73 Å). Final cell constants were obtained from a least-squares fit of a subset of several thousand strong reflections. Data collection was performed by hemisphere runs taking frames at 0.3° (Siemens SMART) and 1.0° (Nonius Kappa-CCD) in ω. Semiempirical absorption corrections using the program SADABS[10] were performed on the data sets of **2**, **3,** and **6**. Intensity data of **4** were not corrected. Crystallographic data of the compounds and diffractometer types used are listed in Table 1. The Siemens ShelXTL[11] software package was used for solution, refinement, and artwork of the structure. The structures were readily solved by direct methods and difference Fourier techniques. All non-hydrogen atoms except some atoms in disordered parts were refined anisotropically, and hydrogen atoms were placed at calculated positions and refined as riding atoms with isotropic displacement parameters. Solvent molecules of crystallization were found to be disordered in all four structures, and disorder of a C_4 chain of the NBu_4 cation in **4** and a *tert*-butyl group in **6** was observed. Split atom models were used to account for the disorder.

Physical Measurements. The equipment and programs for simulations used are the same as described in ref 1. Mössbauer isomer shifts are given relative to iron metal at ambient temperature. EPR microwave power saturation measurements were performed with a Bruker ELEXSYS spectrometer at X-band. Spectra were recorded in 2D mode (intensity vs field vs power), and the temperature which was controlled by an Oxford Instruments cryostat ESR 910 was calibrated by using a standard $S = {}^1/_2$ absorber. Saturation curves were determined from the derivative amplitudes at $g_\perp$.

Results and Discussion

Synthesis of Ligands and Complexes. The ligands 1,2,4,5-tetrakis(2-pyridinecarboxamido)benzene, H_4(tpb), and 1,2,4,5-tetrakis(4-*tert*-butyl-2-pyridinecarboxamido)benzene, H_4(tbpb), have been readily prepared as yellow powders from the reaction of 1,2,4,5-tetraaminobenzene tetrahydrochloride and 4 equiv of picolinic acid and 4-*tert*-butylpicolinic acid, respectively, in pyridine and triphenyl phosphite.

The synthesis of the dinuclear complexes containing the dinucleating tetraanions $(tpb)^{4-}$ and $(tbpb)^{4-}$, respectively, shown in Chart 1 is straightforward. Methanolic solutions of the ligands, 4 equiv of sodium methoxide, 2 equiv of $CoCl_2$·6H_2O, and 4 equiv of NaCN or [N(*n*-Bu)$_4$]CN in the presence of air produced brown-red, diamagnetic microcrystalline materials of Na_2[Co$^{III}_2$(tpb)(CN)$_4$] (**1**) and [N(*n*-Bu)$_4$]$_2$[Co$^{III}_2$(tbpb)(CN)$_4$] (**2**), respectively. The latter species can be electrochemically oxidized in CD_2Cl_2 solution yielding the red neutral complex [Co$^{III}_2$(tbpb^{ox2})(CN)$_4$] (**3**), where diamagnetic $(tbpb^{ox2})^{2-}$ represents the two-electron-oxidized form of the tetraanion $(tbpb)^{4-}$. Similarly, $(tbpb^{ox1})^{3-}$, which is a π−radical ($S_{rad} = {}^1/_2$), represents the one-electron-oxidized form of $(tbpb)^{4-}$.

(10) Sheldrick, G. M. *SADABS*; Universität Göttingen: Göttingen, Germany, 1994.
(11) *ShelXTL*, V.5; Siemens Analytical X-ray Instruments, Inc.: Madison, WI, 1994.

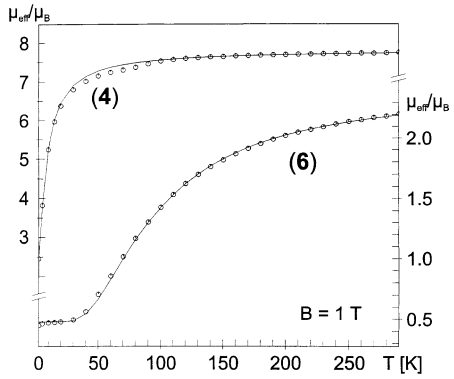

Figure 1. Temperature dependence of the effective magnetic moments of solid **4** (top) and **6** (bottom) at 1 T applied field. The solid lines are simulations based on the spin Hamiltonian $H = -2JS_1S_2 + g\mu_B B(S_1 + S_2)$ with $S_1 = S_2 = {}^5/_2$, $g_{1,2} = 2$ (fixed), and $J = -0.8$ cm^{-1} for **4** and $S_1 = S_2 = {}^1/_2$, $g_{1,2} = 2.03$, and $J = -82$ cm^{-1} for **6**. Paramagnetic impurities from monomeric low-spin contaminations ($S = {}^1/_2$) were considered as PI = 12% for **4** (which is close to a respective component in the 80 K Mössbauer spectrum, $\delta = 0.24$ mm s^{-1}, $\Delta E_Q = 2.24$ mm s^{-1}, 8% relative intensity) and PI = 0.7% for **6**.

The iron-containing complexes $[N(n\text{-}Bu)_4]_2[Fe^{III}{}_2(tpb)(N_3)_4]$ (**4**), $[N(n\text{-}Bu)_4]_2[Fe^{III}{}_2(tpb)(CN)_4]$ (**5**), and $[N(n\text{-}Bu)_4]_2[Fe^{III}{}_2(tbpb)(CN)_4]$ (**6**) were prepared similarly using $FeCl_3 \cdot 6H_2O$, NaN_3, and $[N(n\text{-}Bu)_4]CN$ as starting materials.

In the infrared spectra of complexes **1**−**6** a C≡N stretching frequency of the coordinated cyanide ligands is observed in the narrow range 2109−2134 cm^{-1} (Table S1). The C═O and C═N stretching modes of the coordinated carboxamido part of the bridging ligands are observed in the range 1540−1700 cm^{-1}. Note that the IR spectra of complexes **1**−**6** do not show ν(N−H) vibrations.

The cobalt(III) complexes **1**−**3** are diamagnetic as was judged from their "normal" ^{1}H NMR spectra (see Experimental Section). As expected, the compounds are $3d^6$ low-spin complexes with nonradical ligands.

The iron(III) ions in the azido compound **4** are in the high-spin state as can be inferred from the zero-field Mössbauer spectrum recorded from solid material. At 80 K a narrow quadrupole doublet with typical isomer shift and quadrupole splitting, $\delta = 0.47$ mm s^{-1} and $\Delta E_Q = 0.4$ mm s^{-1}, is observed. Variable-temperature magnetic susceptibility measurements of solid **4** reveal a weak antiferromagnetic exchange interaction of the two iron sites. The effective moment of the molecule is virtually temperature-independent in the range 80−300 K with $\mu_{eff} = 7.4$−$7.8\ \mu_B$, which is close to the spin-only value $8.36\ \mu_B$ for two noninteracting $S = {}^5/_2$ ions with nonmagnetic ligands (Figure 1, top). From a simulation of the measured low-temperature variation at 2−60 K a value of $J \approx -1$ cm^{-1} ($H = -2JS_1 \cdot S_2$, $S_1 = S_2 = {}^5/_2$) was estimated for the spin coupling constant (neglecting zfs). Such weak spin−spin interaction is rather common for ferric high-spin dimers without covalent bridging ligands such as oxo groups.[12]

In contrast, both cyano complexes **5** and **6** contain *low-spin* ferric ions ($S_{Fe} = {}^1/_2$) with typical Mössbauer isomer shift $\delta = 0.11$ mm s^{-1} and the relatively large quadrupole splitting $\Delta E_Q = 1.29$ mm s^{-1}, as measured at 80 K. Surprisingly, the magnetic moment of solid **6** shows a pronounced temperature dependence in the range 50−200 K, revealing strong antiferromagnetic spin coupling and a well isolated diamagnetic ground state of the dimer (Figure 1, bottom). A simulation of the susceptibility data yields a value of $J = -82$ cm^{-1} for the intramolecular coupling constant. EPR spectra of the trisanionic, reduced mixed-valence derivative of **6** given below indicate that here a $3\{d_{xz}{}^2, d_{yz}{}^2, d_{xy}{}^1\}$ configuration is prevailing for the single ferric low-spin ion which means that the magnetic orbitals of the homovalent dimer **6** are the π-bonding d_{xy} orbitals (with respect to the bridging ligand). The strong exchange interaction shows that the aromatic ligand is able to mediate "long-range" spin interaction if the overlap of an extended ligand orbital with the magnetic orbital is large enough.[13] Strong π interaction of the equatorial nitrogen atoms is expected for the low-spin complex because of strong acceptor properties of the electron-deficient ligand system and short iron nitrogen bonds.

In contrast, the high-spin compound **4** exhibits only vanishingly small spin coupling, according to the much lower covalency as it is reflected in the significantly larger average Fe−N bond lengths (1.94 Å for **6**, 2.02 Å for **4**).

To our knowledge, the complexes **4** and **6** represent the first examples of dimeric Fe(III) complexes with an isostructural core for which both a low-spin and a high-spin configuration are available for systematic studies of electronic exchange.

Table 2. Selected Bond Distances (Å)

	2	**3**	**4**	**6**
M−N1	1.984(3)	1.957(2)	2.070(3)	1.989(3)
M−N2	1.894(2)	1.872(2)	1.977(2)	1.885(3)
M−N3	1.970(3)	1.953(2)	2.070(3)	1.999(3)
M−N4	1.892(3)	1.873(2)	1.966(2)	1.887(3)
M−C24	1.925(3)	1.926(3)	1.993(4)	1.970(4)
M−C25	1.930(3)	1.928(3)	2.046(3)	1.971(4)
C21−N4	1.416(4)	1.346(3)	1.409(3)	1.403(4)
C22−N2	1.400(4)	1.353(3)	1.407(4)	1.406(4)
C21−C22	1.410(4)	1.488(3)	1.417(4)	1.417(4)
C21−C23	1.399(4)	1.388(3)	1.402(4)	1.396(4)
C22−C23*	1.406(4)	1.400(3)	1.392(4)	1.398(4)

X-ray Structure Determinations. The structures of complexes $[N(n\text{-}Bu)_4]_2[Co^{III}{}_2(tbpb)(CN)_4]2.8CH_3OH \cdot 1.2H_2O$, $[Co^{III}{}_2(tbpb^{ox2})(CN)_4] \cdot 4CD_2Cl_2$, $[N(n\text{-}Bu)_4]_2[Fe^{III}{}_2(tpb)(N_3)_4] \cdot 3CH_3CN$, and $[N(n\text{-}Bu)_4]_2[Fe^{III}{}_2(tbpb)(CN)_4] \cdot 3.5CH_3OH \cdot 0.5(C_2H_5)_2O$ have been determined by single-crystal X-ray crystallography at 100 K. Table 2 summarizes selected bond lengths. Figure 2 displays the structures of the dianion in **2** (top) and of the neutral species in crystals of **3** (bottom), whereas Figure 3 shows the structures of the dianions in crystals of **4** (top) and **6** (bottom).

As expected, the ligands $(tpb)^{4-}$ or $(tbpb)^{4-}$ in **2**, **4**, and **6** bind two trivalent metal ions (Co^{III} or Fe^{III}), respectively, each via two pyridine and two amido nitrogen donor atoms in the equatorial plane of the octahedral polyhedron around the metal ions. Each metal ion is additionally coordinated

(12) Kurtz, D. M. *Chem. Rev.* **1990**, *90*, 585−606.

(13) Kahn, O. *Molecular Magnetism*; Wiley-VCH Verlag GmbH: Weinheim, Germany, 1993.

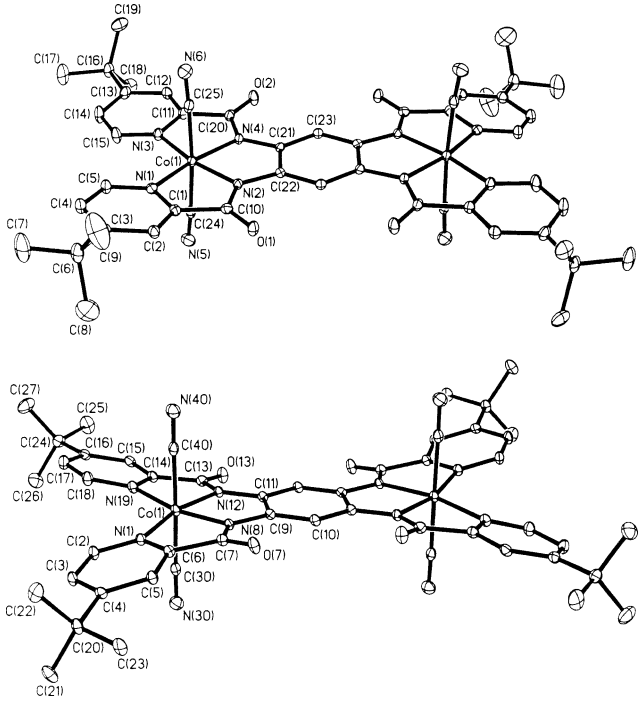

Figure 2. ORTEP representation of the dianion $[Co^{III}_2(tbpb)(CN)_4]^{2-}$ (top) in crystals of **2** and of the neutral complex $[Co^{III}_2(tbpb^{ox2})(CN)_4]$ (bottom) in crystals of **3**.

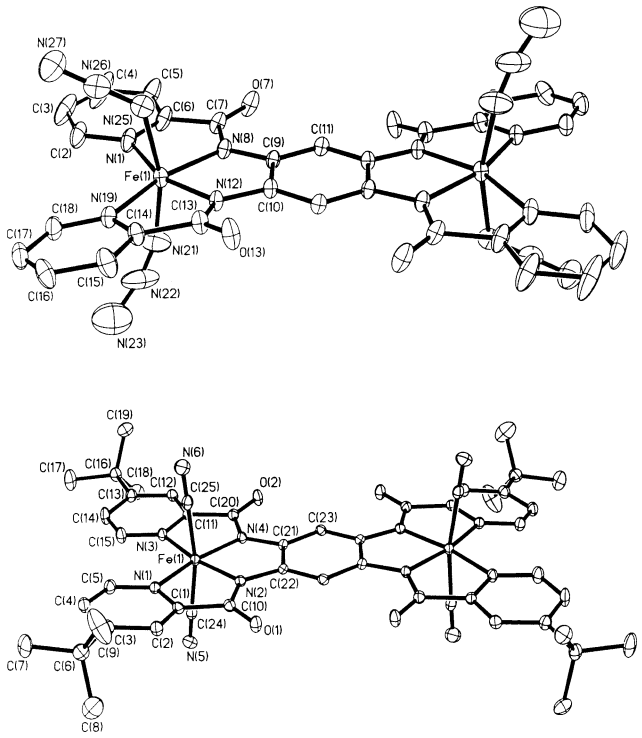

Figure 3. ORTEP representation of the dianion $[Fe^{III}_2(tpb)(N_3)_4]^{2-}$ (top) in crystals of **4** and of the dianion $[Fe^{III}_2(tbpb)(CN)_4]^{2-}$ in crystals of **6**.

to two cyano ligands in trans position relative to each other in **2**, **3**, and **6**. Complex **4** has two monodentate azido ligands in trans position at each iron ion. Interestingly, the $Fe-N_{py}$ and $Fe-N_{amide}$ bond distances are relatively long in **4** but significantly shorter in **6** in agreement with the fact that the former contains high-spin ferric ions whereas in the latter a low-spin ferric configuration prevails.

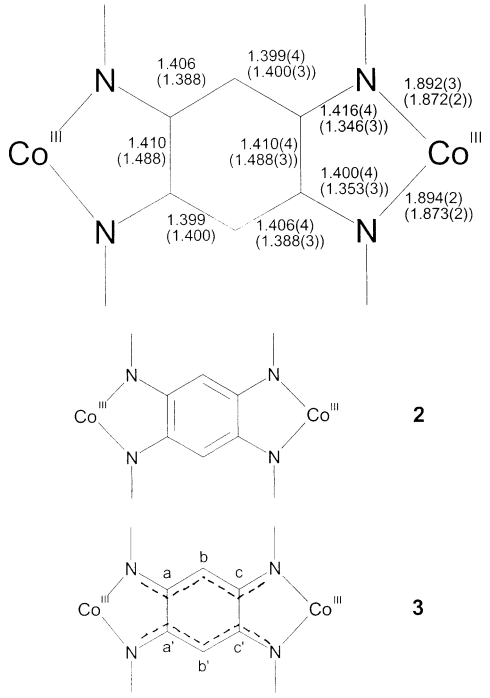

Figure 4. Top: Metrical details of the bridging ligands $(tbpb)^{4-}$ and (in brackets) of $(tbpb^{ox2})^{2-}$ in crystals of **2** and **3**, respectively, and the corresponding resonance structures (middle and bottom).

The most salient feature of these structure determinations is the observation that the two-electron oxidation on going from the dianionic species $[Co^{III}(tbpb)(CN)_4]^{2-}$ in **2** to the neutral analogue $[Co^{III}(tbpb^{ox2})(CN)_4]$ in **3** is clearly ligand centered. Only the dimensions of the central 1,2,4,5-tetraamidobenzene bridging unit differ significantly as shown in Figure 4. The central $N_2(C_6H_2)N_2$ part in complexes **2**, **4**, and **6** displays rather long C−N bonds (average 1.407(3) Å) whereas the corresponding ones in **3** are significantly shorter at 1.350(3) Å indicating considerable double bond character. Similarly, the six C−C bonds are nearly equidistant in **2**, **4**, and **6** indicating that this six-membered ring is an aromatic benzene ring whereas this six-membered ring in **3** shows a severe distortion: the two bonds $C_a-C_{a'}$ and $C_c-C_{c'}$ in Figure 4 are very long at 1.488(3) Å indicating considerable single bond character whereas the four bonds C_a-C_b, $C_{a'}-C_{b'}$, C_b-C_c, and $C_{b'}-C_{c'}$ are significantly shorter at average 1.314 Å. Thus, the bridging unit in **3** must be described as quinone.

Very similar observations have been reported for uncoordinated 1,2,4,5-tetrakis(dimethylamino)benzene and its 2-electron-oxidized form.[14]

Electro- and Spectroelectrochemistry. (a) Oxidation and Reduction Products of the Dinuclear Cobalt(III) Complexes. The electro- and spectroelectrochemistry of complexes **1**, **2** and **5**, **6** have been studied by cyclic and square wave voltammetry and controlled potential coulometry in acetonitrile and dichloromethane solutions containing 0.1 M $[N(n\text{-}Bu)_4]PF_6$ as supporting electrolyte. All potentials are referenced vs the ferrocenium/ferrocene, Fc^+/Fc, couple. The results are summarized in Table 3.

(14) Elbl, K.; Krieger, C.; Staab, H. A. *Angew. Chem.* **1986**, *98*, 1024; *Angew. Chem., Int. Ed. Engl.* **1986**, *25*, 1023.

Table 3. Redox Potentials (V) of Complexes a 20 °C[a]

complex	solvent	$E_{1/2}$,ox2[b]	$E_{1/2}$,ox1[c]	$E_{1/2}$,red1[d]	$E_{1/2}$,red2[e]
1	CH_3CN	0.287	−0.118	∼ −2 (irr)	
2	CH_3CN	0.29	−0.12	∼ −2 (irr)	
	CH_2Cl_2	0.17	−0.23	∼ −1.9 (irr)	
5	CH_3CN	0.64	−0.24	−1.31	−1.41
6	CH_2Cl_2	0.54	−0.33		
	CH_3CN	0.64	−0.24	−1.31	−1.41

[a] Conditions: glassy carbon working electrode, 0.01 M $Ag/AgNO_3$ in CH_3CN reference electrode; 0.1 M $[N(n\text{-}Bu)_4]PF_6$ supporting electrolyte; all potentials are referenced vs F_c^+/F_c (internal standard). [b] Redox potentials for the couple $[complex]^{0/-}$. [c] For the couple $[complex]^{-/2-}$. [d] For the couple $[complex]^{2-/3-}$. [e] For the couple $[complex]^{3-/4-}$. irr = irreversible reduction wave $Co^{III} \rightarrow Co^{II}$.

Both cobalt complexes **1** and **2** display each two reversible one-electron oxidation waves and at very negative potentials below −1.8 V an irreversible metal-centered reduction which was not further studied, eq 2. Spectral changes during the two successive one-electron oxidations of **2** were monitored by spectroelectrochemical methods where the monoanion of **2** and the neutral complex **3** were generated by controlled potential coulometry. Figure 5 shows the spectra of the di- and monoanion as well as that of the neutral form **2**, and Table S2 summarizes the spectra. These spectra clearly show that both oxidations are ligand- rather than metal-centered:

$$[Co^{III}{}_2(tbpb)(CN)_4]^{2-} \underset{+e}{\overset{-e}{\rightleftharpoons}} [Co^{III}{}_2(tbpb^{ox1})(CN)_4]^{-} \underset{+e}{\overset{-e}{\rightleftharpoons}} [Co^{III}{}_2(tbpb^{ox2})(CN)_4]^{0} \quad (1)$$

$$E_{1/2},ox1 \qquad E_{1/2},ox2$$

Thus, the monoanions $[Co^{III}{}_2(tpb^{ox1})(CN)_4]^-$ and $[Co^{III}{}_2(tbpb^{ox1})(CN)_4]^-$ are expected to be paramagnetic with an $S = {}^1/_2$ ground state. This is indeed the case as was demonstrated by their X-band EPR spectra recorded at ambient temperature. Figure 6 shows the spectrum of electrochemically generated $[Co^{III}{}_2(tpb^{ox1})(CN)_4]^-$ in CH_3CN (0.1 M $[N(n\text{-}Bu)_4]PF_6$). That of $[Co^{III}{}_2(tbpb^{ox1})(CN)_4]^-$ in CH_2Cl_2 is virtually identical and not shown. The spectrum exhibits an $S = {}^1/_2$ signal at $g = 2.002$ with a 15 line hyperfine splitting to two equivalent ^{59}Co ($I = {}^7/_2$) nuclei ($A(^{59}Co) = 15.2$ MHz with an isotropic line width of 0.31 mT). Superhyperfine splitting to nitrogens or protons has not been resolved. The simulation shown in Figure 6 takes into account some microinhomogeneity of the sample in solution by using a quadratic *A*-strain parameter $C_{Co} = 0.2$ MHz. From the observation of a single ^{59}Co-hyperfine coupling constant to two equivalent Co^{III} ions it follows unequivocally that the unpaired electron resides in a π−orbital of a semiquinonate radical with some covalent admixture from both Co^{III} sites.

As shown in Figure 5 the oxidation of the bridging semiquinonate in $[Co^{III}{}_2(tbpb^{ox1})(CN)_4]^-$ to the quinone in $[Co^{III}(tbpb^{ox2})(CN)_4]^0$ (**3**) is accompanied by the disappearance of the π−radical charge transfer (CT) bands in the range 750 to 1100 nm and the appearance of quinone CT bands in the region 600−800 nm.

(b) Reduction Products of the Dinuclear Iron(III) Complexes. Figure 7 shows the CV of **6** (that of **5** is very similar and not shown). Clearly, two well-resolved, reversible

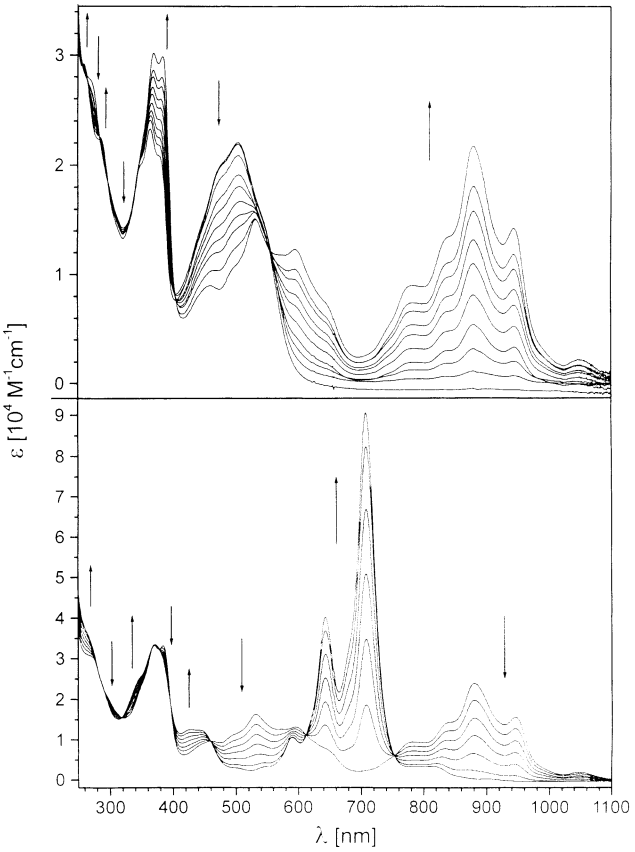

Figure 5. Top: Spectroelectrochemical oxidation of **2** in CH_2Cl_2 (0.1 M $[TBA]PF_6$) to the corresponding monoanion $[Co^{III}{}_2(tbpb^{ox1})(CN)_4]^-$ at 248 K. Bottom: Oxidation of the monoanion to the neutral species $[Co^{III}{}_2(tbpb^{ox2})(CN)_4]^0$ (conditions as above).

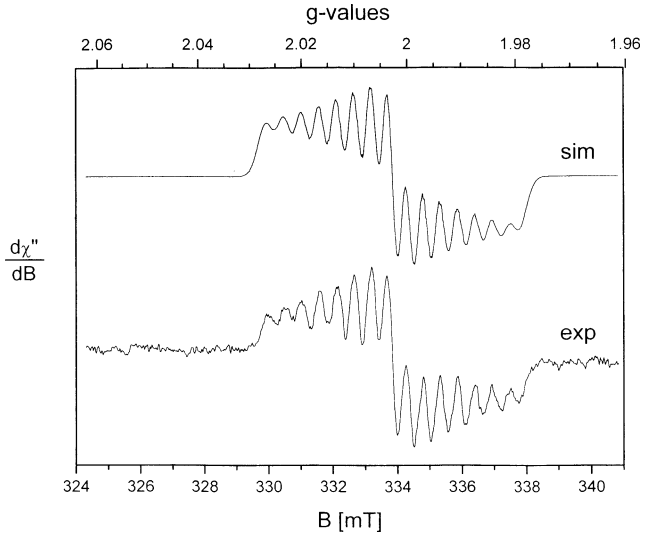

Figure 6. X-band EPR spectrum of electrochemically generated $[Co^{III}{}_2(tpb^{ox1})(CN)_4]^-$ (monooxidized **1**) in CH_3CN at 298 K (0.1 M $[TBA]PF_6$). Conditions: frequency, 9.452 GHz; microwave power, 2 mW; modulation frequency, 100 kHz; modulation amplitude, 0.2 mT. Simulation parameters: see text.

1-electron oxidation waves and two closely related 1-electron reduction waves are observed in CH_3CN and CH_2Cl_2 solutions. In the following we have only studied complex **6** in detail due to its better solubility in organic solvents. As we will show, subsequently the 1-electron oxidations and reductions of **6** yield the species shown in Scheme 1.

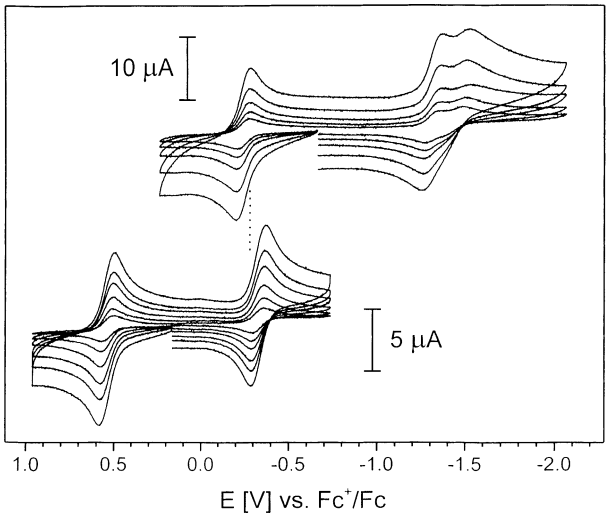

Figure 7. Cyclic voltammogram of **6** in CH_3CN (0.1 M $[TBA]PF_6$) (top trace) and in CH_2Cl_2 (0.1 M $[TBA]PF_6$) (bottom trace) at 295 K at scan rates 50, 100, 200, 400, 600 (only in CH_2Cl_2 solution), and 800 mV s^{-1} at a glassy carbon working electrode.

Scheme 1. One-Electron-Interrelated Species of **6**

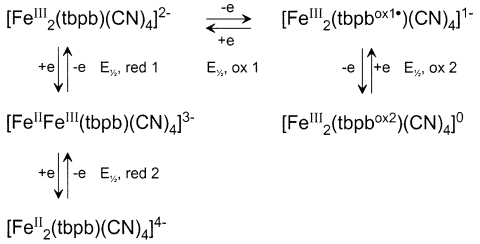

Since the redox potentials $E_{1/2}$,red1 and $E_{1/2}$,red2 differ by only 97 mV, it is not possible to generate the pure trianion $[Fe^{III}Fe^{II}(tbpb)(CN)_4]^{3-}$ in solution because it disproportionates (see below). Therefore, we have reduced **6** by two electrons electrochemically and recorded the electronic absorption spectrum of the tetraanion of **6** which is shown in Figure 8. It is remarkable how similar the spectra of the tetraanion of **6** and of isoelectronic **2** are (Figure 5). This leads immediately to the conclusion that this reduction of **6** is metal-centered yielding two low-spin ferrous ions (d^6). In agreement with this the tetraanion is EPR silent ($S = 0$).

The electrochemical 2-electron reduction of **6** was also monitored in the infrared by using an OTTLE cell. Complex **6** displays two ν(C≡N) stretching frequencies in CH_2Cl_2 solution at 2118 and 2110 cm^{-1} whereas the fully reduced tetraanion displays a single ν(C≡N) frequency at 2051 cm^{-1}. This shift is in excellent agreement with the notion that two low-spin ferric ions in **6** are reduced to two equivalent low-spin ferrous ions. These experiments did not allow the observation of the so far elusive mixed-valence trianion $[Fe^{II}Fe^{III}(tbpb)(CN)_4]^{3-}$.

In an attempt to characterize the mixed-valent trianion we have calculated the comproportionation constant, K_c, for the equilibrium, eq 2, by using the relation eq 3, where ΔE is the difference of ($E_{1/2}$,red1 − $E_{1/2}$,red2) = 97 mV. It is now possible to calculate the maximum concentration accessible of the trianion. This result is depicted in the inset of Figure 9. Thus, mixing two equimolar solutions of the tetra- and the dianion yields a solution which contains 46.5% of the tetra- and 46.5% of the dianion and only 7% of the mixed-valent trianion. The experimentally accessible concentration of the trianion in solution is therefore rather small.

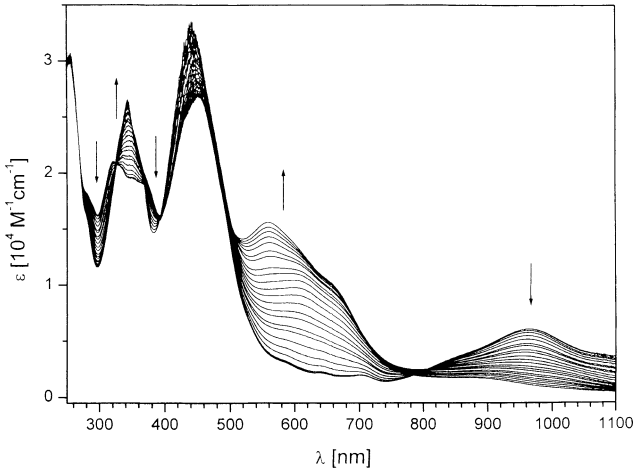

Figure 8. Spectral changes during the coulometric 2e reduction of **6** to $[Fe^{II}_2(tbpb)(CN)_4]^{4-}$ in CH_2Cl_2 (0.1 M $[TBA]PF_6$) at 248 K.

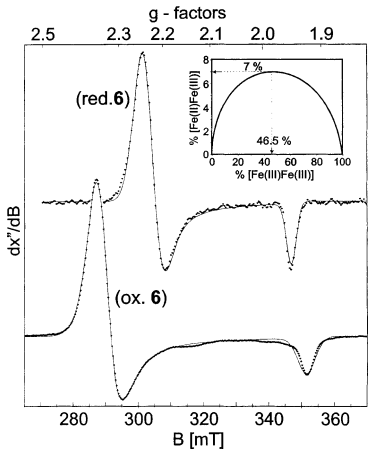

Figure 9. X-band EPR spectra of electrochemically reduced and oxidized compound **6** in CH_3CN (1 mM [**6**], 0.1 M $[TBA]PF_6$, 1e/molecule reduced or oxidized). Experimental conditions (bottom/top): microwave frequency, 9.4650 GHz/9.4668 GHz; power, 1 μW/3.6 μW; modulation (100 kHz), 1 mT/1 mT. Inset: yield of mixed-valent complex $[Fe^{III}Fe^{II}(tbpb)(CN)_4]^{3-}$ (reduced **6**). The solid lines are fits of simulated powder spectra with g values as given in the text and Table 6.

$$2[Fe^{II}Fe^{III}(tbpb)(CN)_4]^{3-} \underset{K_c}{\rightleftharpoons} [Fe^{II}_2(tbpb)(CN)_4]^{4-} + [Fe^{III}_2(tbpb)(CN)_4]^{2-} \quad (2)$$

$$K_c = 10\exp\left(\frac{\Delta E}{59\text{ mV}}\right) = 44 \quad (3)$$

Since the tetra- and the dianion are diamagnetic at low temperatures (<20 K), it should be possible to detect the signal of the paramagnetic trianion ($S = {}^1/_2$) by EPR spectroscopy. This is indeed the case as shown in Figure 9 which shows the X-band EPR spectrum of a CH_2Cl_2 solution (0.1 M $[N(n\text{-}Bu)_4]PF_6$) of **6** which had been electrochemically reduced by exactly one electron/dinuclear ion of **6**. Clearly, an axial $S = {}^1/_2$ signal at $g_\perp = 2.23$ and $g_\parallel = 1.95$ is observed. The large g-anisotropy is typical for a low-spin ferric ion. Quantitation of this signal revealed that 5−8% of the starting

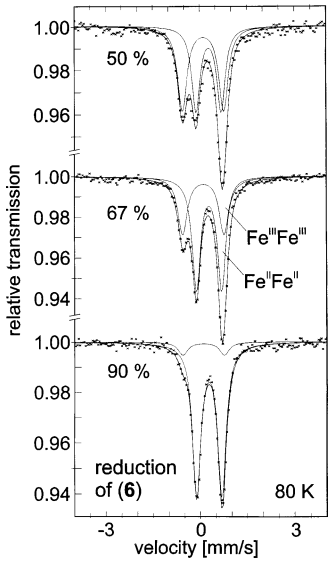

Figure 10. Zero-field Mössbauer spectra of 50%, 67%, and 90% coulometrically reduced compound **6** in acetonitrile solution. The lines are fits with Lorentzian doublets with equal parameters as given in Table 6 and variant relative intensities, with $[Fe^{III}Fe^{III}]$:$[Fe^{II}Fe^{II}]$ = 53:47, 37:63, and 9:91 (top to bottom).

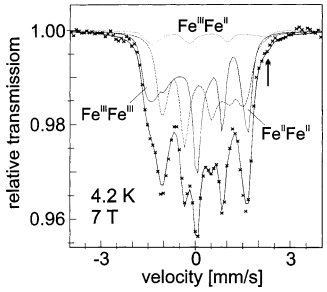

Figure 11. Magnetic Mössbauer spectrum of the 50% coulometrically reduced compound **6** (see Figure 10 top) at 4.2 K with 7 T field applied perpendicular to the γ-rays. The lines are spin Hamiltonian simulations with $S = 0$ for the homovalent species $Fe^{III}Fe^{III}$ and $Fe^{II}Fe^{II}$ and $S = {}^1/_2$ for the mixed-valent minority $Fe^{III}Fe^{II}$ and parameters as given in the text.

complex **6** had been converted to the EPR-active trianion $[Fe^{II}Fe^{III}(tbpb)(CN)_4]^{3-}$, which is in excellent agreement with the above calculated amount of 7%. Since the Mössbauer data below indicate localized valences for the trianionic mixed-valent reduction product of **6**, it is clear that the EPR *g* values probe selectively the electronic structure of the ferric site of the $Fe^{II}Fe^{III}$ dimer, because the ferrous site is low-spin ($S = 0$) and does not contribute to the paramagnetic properties of the molecule. An interpretation of the data is presented below in conjunction with those of the oxidation products of **6**.

We have also recorded the zero- and applied field Mössbauer spectra of frozen CH_3CN solutions of **6** (0.10 M $[N(n\text{-}Bu)_4]PF_6$) which were electrochemically reduced by two electrons/dinuclear unit to (a) 50%, (b) 67%, and (c) 90%. The spectra are shown in Figure 10, and the results are summarized in Table 4. As noted above, the dianion **6**, $[Fe^{III}{}_2(tbpb)(CN)_4]^{2-}$, possess an $S_t = 0$ ground state obtained via weak antiferromagnetic coupling of two low-spin ferric ions and, consequently, the zero-field Mössbauer spectrum of **6** displays a single quadrupole doublet with isomer shift, δ, of 0.10 mm s^{-1} and $|\Delta E_Q| = 1.31$ mm s^{-1} quadrupole splitting. Similarly, the zero-field spectrum of the fully reduced diamagnetic tetraanion, $[Fe^{II}{}_2(tbpb)(CN)_4]^{4-}$, displays a single quadrupole doublet with $\delta = 0.29$ mm s^{-1} and $\Delta E_Q = 0.80$ mm s^{-1} which is quite typical for an octahedral low-spin ferrous ion. The one-electron reduced mixed-valence dimer is virtually not detectable in the zero-field Mössbauer spectra of the reduced material at 80 K. In a wide range of coulometric yields the spectra can be readily fitted with only two symmetric Lorentzian doublets with the parameters for $Fe^{II}Fe^{II}$ and $Fe^{III}Fe^{III}$. This means that the valences of the $Fe^{II}Fe^{III}$ dimer are localized and the individual iron sites are virtually independent with Mössbauer parameters that are not discernible from those of the respective homovalent Fe^{II}-Fe^{II} and $Fe^{III}Fe^{III}$ dimers. (The interpretation assumes that the paramagnetic relaxation of the $Fe^{II}Fe^{III}$ dimers is fast on the Mössbauer time scale and possible magnetic splittings of the Mössbauer spectrum are collapsed, which is reasonable for zero-field spectra at 80 K.)

In the magnetically perturbed spectra at liquid-helium temperatures, the presence of the mixed-valence species is indicated by a weak shoulder outside the range of the major diamagnetic subspectra, marked by an arrow in Figure 11. Therefore, a third component comprising 6% of the total iron (at 50% coulometric reduction) was invoked in the magnetic Mössbauer simulations. It is superimposed to the two major diamagnetic components from the homovalent dimers. Due to the low concentration of this species it has not been possible to accurately fit the parameters δ, ΔE_Q, line width Γ, hyperfine tensor A, and electric field gradient η for this anion. Since this component is believed to be the mixed-valent trianion $[Fe^{II}Fe^{III}(tbpb)(CN)_4]^{3-}$, we have used the parameters of the low-spin ferric ion as obtained previously for the mononuclear $[Fe^{III}(bpb)(CN)_2]^-$ anion.[1] The spectrum of the low-spin ferrous ion assumed to be diamagnetic and the same as in $[Fe^{II}2(tbpb)(CN)_4]^{4-}$. These assumptions are justified and yield a very satisfactory fit of the data because in the trianion the valences are localized. Thus, the Mössbauer spectrum of a 1:1 mixture of the tetra- and dianion of **6** exhibits ~6% of the trianion in excellent agreement with the EPR results. Furthermore, it clearly follows from this

Table 4. Mössbauer Parameters of Oxidized and Reduced Species of **6**

complex	S[a]	δ, mm s^{-1} [b]	ΔE_Q, mm s^{-1} [c]	ν(CN), cm^{-1} [d]	*g*-values[e]
$[Fe^{II}{}_2(tbpb)(CN)_4]^{4-}$	0	0.29	0.80	2051	
$[Fe^{II}Fe^{III}(tbpb)(CN)_4]^{3-}$	$^1/_2$				2.23 ($g_\perp$), 1.95 ($g_\parallel$)
$[Fe^{III}{}_2(tbpb)(CN)_4]^{2-}$	0	0.10	−1.31	2118, 2110	
$[Fe^{III}{}_2(tbpb^{ox1})(CN)_4]^-$	$^1/_2$	0.07	−1.31	2125, 2118	2.34 ($g_\perp$), 1.92 ($g_\parallel$)
$[Fe^{III}{}_2(tbpb^{ox2})(CN)_4]^0$	0	0.04	−1.30		

[a] Ground state. [b] Isomer shift vs α-Fe at 295 K. [c] Quadrupole splitting. [d] ν(C≡N) stretching frequencies. [e] From X-band EPR spectra.

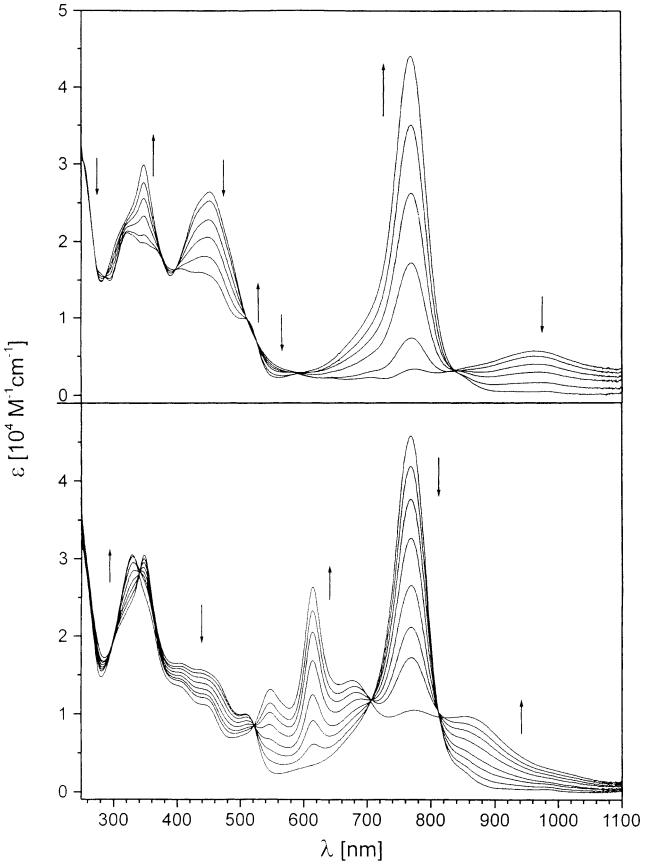

Figure 12. Top: Spectral changes during the coulometric 1e oxidation of **6** to $[Fe^{III}_2(tbpb^{ox1})(CN)_4]^-$. Bottom: Spectral changes during the coulometric 1e oxidation of $[Fe^{III}_2(tbpb^{ox1})(CN)_4]^-$ to the neutral species $[Fe^{III}_2(tbpb^{ox2})(CN)_4]^0$. Conditions: CH_2Cl_2 solution (248 K; 0.1 [TBA]-PF_6).

study that the reductions of **6** are metal-centered; the low-spin ferric ions are reduced to low-spin ferrous ions.

(c) Oxidation Products of the Dinuclear Iron(III) Complexes. In a completely analogous fashion we have studied the oxidation products of **6**, namely the monoanion $[Fe^{III}_2(tbpb^{ox1})(CN)_4]^-$ ($S_t = {}^1/_2$) and neutral $[Fe^{III}_2(tbpb^{ox2})(CN)_4]^0$ ($S_t = 0$).

Figure 12 shows the electronic spectrum of the electrochemically generated monoanion and of the neutral species of **6**, respectively. Table S2 summarizes these measurements. The new intense absorption band at 768 nm of the monoanion is remarkable since it disappears again upon oxidation to the neutral species which displays a similar new transition at 614 nm. Note that quite similar behavior has been observed for the spectra of the cobalt complexes $[Co^{III}_2(tbpb^{ox1})(CN)_4]^-$ and $[Co^{III}_2(tbpb^{ox2})(CN)_4]^0$. This indicates that both oxidations of **6** are ligand-centered processes. In agreement with this interpretation is the observation that the two ν(C≡N) stretching frequencies of **6** are shifted only by 7−8 cm^{-1} to higher energy at 2125 and 2118 cm^{-1} (Table 4). Thus the coordinated CN^- ligands do not experience an increase of the oxidation state of the ferric ions on going from the di- to the monoanion. Note that upon reduction of **6** to the tetraanion a shift of 59 or 67 cm^{-1} is observed due to the reduction of two ferric to two ferrous ions.

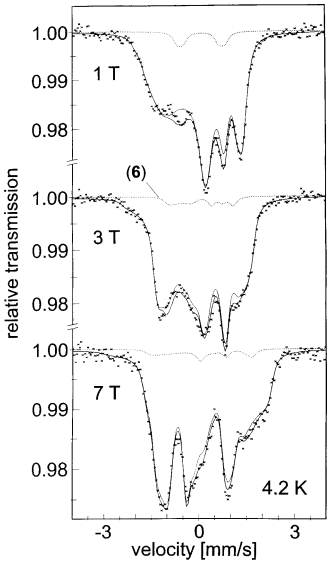

Figure 13. Magnetic Mössbauer spectra of the oxidized complex $[Fe^{III}_2(tbpb^{ox1})(CN)_4]^-$ at 4.2 K with applied fields as indicated applied perpendicular to the γ-rays. The solid lines are spin Hamiltonian simulations with $S = {}^1/_2$ for the major product. The dotted line represents a simulation of 5% residual starting complex **6** with $S = 0$.

Table 5. Spin Multiplets of the Spin-Coupled System $[Fe^{III}_2(tbpb^{ox1})(CN)_4]^-$ (Oxidized **6**)

(S_t,S^*)	energy	$\mathbf{g}_t$[a]
(3/2,1)	$-3J$	$\mathbf{g}_t = 2/3\mathbf{g}_{Fe} + 1/3\mathbf{g}_{rad}$
(1/2,0)	$-2J + 2J'$	$\mathbf{g}_t = \mathbf{g}_{rad}$
(1/2,1)	0	$\mathbf{g}_t = 4/3\mathbf{g}_{Fe} - 1/3\mathbf{g}_{rad}$

[a] **g** matrix of the total spin S_t.

Since the monoanion contains an uneven number of electrons, we have recorded its X-band EPR spectrum at 10 K which is shown in Figure 9. An axial $S = {}^1/_2$ signal is observed with $g_\perp = 2.34$ and $g_\parallel = 1.92$. Thus, the monoanion possesses an $S_t = {}^1/_2$ ground state which results from the antiferromagnetic interaction of two low-spin ferric ions ($S_{Fe} = {}^1/_2$) and a ligand π-radical $(tbpb^{ox1\bullet})^{3-}$ ($S_{rad} = {}^1/_2$). The nature of this three-spin system will be discussed below in more detail.

The applied field Mössbauer spectra of the monoanion $[Fe^{III}_2(tbpb^{ox1})(CN)_4]^-$ are shown in Figure 13. The applied-field spectra confirm the $S_t = 0$ ground state for the neutral species $[Fe^{III}_2(tbpb^{ox2})(CN)_4]^0$ and an $S_t = {}^1/_2$ for the corresponding monoanion. The iron sites of both dinuclear species are indistinguishable, and the spectra have been successfully simulated by using the parameters given in Tables 4 and 6. It is noteworthy that the isomer shifts δ at 80 K of **6**, its monoanion, and its dianion of 0.10, 0.07, and 0.04 mm s^{-1} decrease barely significantly by 0.06 mm s^{-1} with decreasing overall charge from 2−, to 1−, to 0, respectively. The quadrupole splitting parameter is negative and nearly invariant at ∼1.3 mm s^{-1}. This result clearly indicates that the oxidation states of the iron ions in the di- and monoanion and neutral species are the same, namely low-spin ferric. Noticeably, the monoanion is *not* a mixed-valent complex.

(d) Electronic Structure of $[Fe^{III}_2(tbpb^{ox1})(CN)_4]^-$. As we have shown above, the monoanion $[Fe^{III}_2(tbpb^{ox1})(CN)_4]^-$

Table 6. Comparison of EPR g-Values and ^{57}Fe Hyperfine Tensor of the Reduction and the Oxidation Product of **6**[a]

	$[Fe^{III}Fe^{II}(tbpb)(CN)_4]^{3-}$ (reduced **6**)	$[Fe^{III}_2(tbpb^{ox1})(CN)_4]^-$ (oxidized **6**)
$g_{x,Fe}$	2.233	2.254 (2.338 exptl)
$g_{y,Fe}$	2.233	2.251 (2.335 exptl)
$g_{z,Fe}$	1.951	1.942 (1.922 exptl)
$A_{x,Fe}/g_N\beta_N$	*b*	+6.3 T (+8.4 T exptl)
$A_{y,Fe}/g_N\beta_N$	*b*	−3.3 T (−4.4 T exptl)
$A_{z,Fe}/g_N\beta_N$	*b*	−12.4 T (−16.5 T exptl)

[a] The $g_{i,Fe}$, $i = x, y, z$, represent the components of the local g matrix of the iron(III) low-spin sites that are converted from the experimental values (in parentheses) by using the relation $g_{exp} = {}^4/_3 g_{Fe} - {}^1/_3 g_{rad}$ in the case of oxidized **6** and $g_{exp} = g_{Fe}$ for reduced **6**. $A_{i,Fe}/g_N\beta_N$ are the local **A** tensor components that were converted by using the same relations. [b] Not determined because of low yield.

Scheme 2. Coupling Arrangement for $[Fe^{III}_2(tbpb^{ox1})(CN)_4]^-$

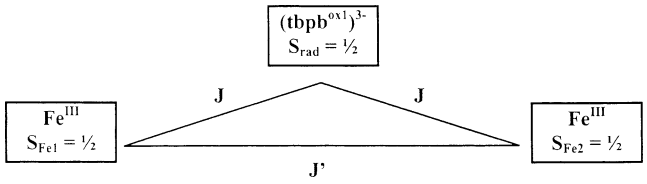

possesses an $S_t = {}^1/_2$ ground state which is composed of two low-spin ferric ions and a bridging π-radical ligand, $(tbpb^{ox1})^{3-}$. In the three-spin system, two total spin doublet states and a spin quartet state are generated by spin coupling[13,15] and the nature of the ground state depends on the relative coupling strengths as shown in Table 5. An "isosceles" interaction topology has been adopted for the symmetric monoanion of oxidized **6** as sketched in Scheme 2, and the energies of the spin multiplets (Table 5) are obtained from the corresponding coupling Hamiltonian:

$$H = -2J(\mathbf{S}_{Fe1} + \mathbf{S}_{Fe2})\cdot\mathbf{S}_{rad} - 2J'\mathbf{S}_{Fe1}\cdot\mathbf{S}_{Fe2} \qquad (4)$$

The three molecular spin multiplets $\{S_t, S^*\}$ are labeled by the total spin $S_t = S_{Fe1} + S_{Fe2} + S_{rad}$ and the hypothetical "intermediate" spin $S^* = S_{Fe1} + S_{Fe2}$. The doublet ($S_t = {}^1/_2$, $S^* = 0$) is the ground state if strong antiferromagnetic interaction between the iron sites dominates the iron-radical interactions ($|J'| > |J|$). In the opposite situation, $|J| > |J'|$, the other doublet ($S_t = {}^1/_2$, $S^* = 1$) is the ground state (provided that the intrinsic interactions are both antiferromagnetic), as shown in Table 5. The possible ground states can be distinguished from the EPR spectra because the respective g values are different due to different parentship from the radical and iron spins (see Table 5) and because the ferric low-spin ions contribute large anisotropic $\mathbf{g}_{Fe}$ matrices. Since the experimental EPR spectrum of oxidized **6** shows a pronounced g anisotropy, $\mathbf{g}_t = (2.338, 2.335, 1.922)$, see Figure 9 (bottom), the spin ground state of the molecule must be given by the doublet ($S_t = {}^1/_2$, $S^* = 1$) with a molecular g value $\mathbf{g}_t = {}^4/_3\,\mathbf{g}_{Fe} - {}^1/_3\,\mathbf{g}_{rad}$. For the other doublet antiparallel spin orientation would virtually "cancel" the influence of the local iron spins, $\mathbf{g}_t = \mathbf{g}_{rad}$, and the isotropic paramagnetic behavior of the ground state would be expected. By using the experimental g values of the monoanion and assuming an isotropic value for the radical $g_{rad} = 2.002$, the total g value yields an estimate of the single ion g values of the ferric ions. Provided that the excited doublet is high in energy and does not mix with the ground state, and the ferric ions have coinciding principal axes systems, one obtains local values $\mathbf{g}_{Fe} = (2.254, 2.251, 1.942)$ which are strikingly close to $\mathbf{g}_{Fe} = (2.23, 2.23, 1.95)$ as measured for the ferric site in the mixed-valence dimer of the first *reduction* product of **6** (Figure 9) for which the ferrous site is low spin and nonmagnetic. We conclude that in fact the adopted relation of local and total g values is valid for oxidized **6** (because the doublets are well separated and hardly mix), and the electronic structures of the ferric ions in the reduced mixed-valence trianion and in the oxidized monoanion are virtually identical.

An interpretation of the local g_{Fe} values of low-spin ferric iron in the oxidation, as well as in the reduction product of **6** (and presumably in the dianion **6** itself), can be derived from the crystal-field model developed by Griffith[16] for the description of the spin−orbit interaction of distorted $(t_{2g})^5$ complexes with a $(d_{xz}, d_{yz})^4(d_{xy})^1$ electron configuration. The best ligand field parameters that can be obtained for the monoanion by using Taylors[17] "proper axes" system ($V < 2/3\Delta$) impose a relatively large axial splitting to the t_{2g} orbital set, $\Delta/\lambda = -7.7$, with a weak rhombic distortion, $V/\lambda = 0.1$. This splitting scheme implies strong antibonding π-interaction of the iron d_{xy} orbital with the *in-plane* p_x and p_y orbitals of the tbpb-N ligand atoms which apparently are stronger π-acceptors than the cyano ligands and shift d_{xy} above d_{xz}/d_{yz}.

The magnetic Mössbauer spectra of oxidized **6**, $[Fe^{III}_2(tbpb^{ox1})(CN)_4]^-$ (Figure 13), strongly support the description of the ferric iron in **6** and its redox derivatives as low-spin Fe(III) complexes with a destabilized d_{xy} orbital in the t_{2g} orbital set. The anisotropy of the valence electrons caused by the electron *hole* in the d_{xy} orbital is expected to induce a strong *negative* valence contribution to the main component of the efg in the z-direction (and a small asymmetry parameter), in accordance with the experimental observation. The asymmetry of the experimental magnetic hyperfine tensor **A** is also consistent with the d_{xy}-hole picture. The orbital coefficients in this model lead to strong orbital and spin-dipolar contributions to **A** which explain the large, negative A component in the direction of the efg main component.[18] The best solution for the local $\mathbf{A}_{Fe}$ tensor that can be obtained in the ligand-field picture (with $\kappa = 0.3$, $P = 17.3$ T) is $\mathbf{A}_{Fe}/g_N\beta_N = (+3.6, -3.7, -13)$ T, which is very close to the experiment. Hence, the magnetic Mössbauer spectra support the description of $[Fe^{III}_2(tbpb^{ox1})(CN)_4]^-$ as a system with $(d_{xz}, d_{yz})^4(d_{xy})^1$ electron configuration of the ferric ions with destabilized d_{xy} orbital in the t_{2g} orbital set due to dominant π-interaction of the tbpb ligand.

The total splitting of the molecular spin states is determined by the values of the coupling constants J and J' for

(15) Bencini, A.; Gatteschi, D. *EPR of Exchange Coupled Systems*; Springer-Verlag: Berlin, 1990.

(16) Griffith, J. S. *Prog. R. Soc. London, A* **1956**, *235*, 23−36.
(17) Taylor, C. P. S. *Biochim. Biophys. Acta* **1977**, *491*, 137−149.
(18) Oosterhuis, W. T.; Lang, G. *Phys. Rev.* **1969**, *178*, 439−456.

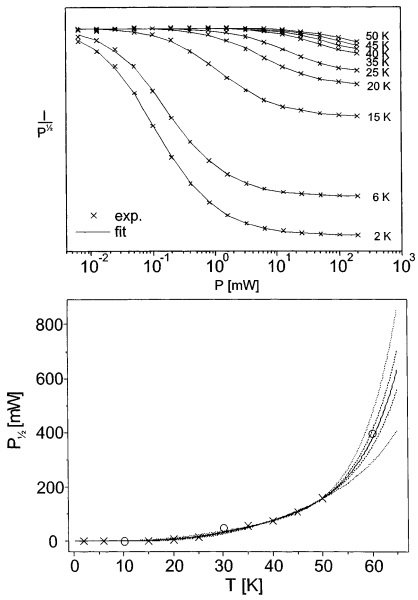

Figure 14. Temperature variation of EPR half-saturation power $P_{1/2}$ of oxidized complex $[Fe^{III}_2(tbpb^{ox1})(CN)_4]^-$ (X-band spectra; see Figure 9) and values calculated by using eq 6. The solid line is a best fit obtained with parameters $a = 0$, $b = 2.2 \times 10^{-14}$ K^{-9} s^{-1}, $c = 8.6 \times 10^{-4}$ cm^3 s^{-1}, and $\Delta = 99$ cm^{-1}; the dashed and dotted lines mark error ranges calculated with $\Delta = 99$ cm$^{-1} \pm 10$ cm^{-1} and ± 30 cm^{-1}, respectively (other parameters independently reoptimized). Inset: Power saturation curves measured at different temperatures and calculated by using eq 6.

the iron−radical and the iron−iron interaction as shown in Table 5. If the energy of the ground state doublet (1/2,1) is set to zero, the excited multiplets are found at energies $-J + 2J'$ (1/2,0) and $-3J$ (3/2,1). Since we can adopt negative values for both J and J', it is clear that for $[Fe^{III}_2(tbpb^{ox1})(CN)_4]^-$ the spin quartet state is highest in energy. We probed the separation of the low-lying spin doublet states by EPR power saturation measurements and their interpretation with spin relaxation mechanism via the first excited spin state (Orbach process).[19] To this end X-band EPR spectra were measured with variable power in the temperature range 2−50 K and the saturation behavior was simulated by using

$$I = I_{max}\sqrt{P}/(1 + P/P_{1/2})^{\beta/2} \quad (5)$$

where I is the EPR intensity (amplitude of the derivative spectra) and $P_{1/2}$ is the power for half-saturation.[20] $P_{1/2}$ correspond to the T_1 relaxation rates, $P_{1/2} \propto 1/T_1$. The temperature dependence of the half-saturation value was fitted by using

$$P_{1/2} = aT + bT^9 + c\Delta^3 e^{\Delta/kT} \quad (6)$$

to account for direct, Raman- and Orbach-type processes.[19,20] These measurements and the fit are shown in Figure 14.

Because of the exponential behavior of the Orbach process, the influence of the high-lying spin quartet state was discarded for relaxation within the ground-state doublet. The nonlinear variation of the half-saturation values indicates that in fact an Orbach-type relaxation process is effective for the monoanion. The best value for the energy gap Δ was obtained from a least-squares optimization $\Delta = 99$ cm^{-1}. However, a large error interval of about ± 30 cm^{-1} has to be taken into account, as estimated from systematic variations of Δ and fitting of the other parameters. Important is the observation that the excited state is found at moderate energies, which means that the iron−radical coupling constants J should not be excessively strong with respect to thermal measurements.

If the value of the iron−iron exchange coupling constant $J' = -82$ cm^{-1} that was found for the dianion **6** can be taken as a reasonable estimate for the iron−iron interaction in the oxidized complex (provided that the increased electron deficiency of the oxidized ligand does not induce much enhanced π-bonding), the iron−radical coupling can be assessed from the relation $\Delta = -2J + 2J'$ to be $J \approx -130$ cm^{-1}. This value is very similar to that of the "long-range" iron−iron interaction through the ligand. It is interesting to speculate about different coupling mechanisms for the iron−iron and the iron−radical interactions. Whereas the first, as stated above, owes its strength to strong π-interaction of the iron magnetic d_{xy} orbital and the *in-plane* nitrogen p_x and p_y orbitals that are "propagated" like σ-type orbitals through the ligand, the iron−radical coupling results from π interaction of the *out-of-plane* nitrogen p_z orbitals (π-radical) with the iron d_{xz} and d_{yz} orbitals which carry only minor spin density due to the spin−orbit mixing with the basic d_{xy} magnetic orbital.

Conclusion

We have shown in this study that the dinucleating tetraanions of the ligands 1,2,4,5-tetrakis(2-pyridinecarboxamido)benzene, H_4(tpb), and 1,2,4,5-tetrakis(4-*tert*-butyl-2-pyridinecarboxamido)benzene, H_4(tbpb), can exist in two one-electron-oxidized forms, namely the π-radical trianions, $(tpb^{ox1\bullet})^{3-}$ and $(tbpb^{ox1\bullet})^{3-}$, and the diamagnetic dianions, $(tpb^{ox2})^{2-}$ and $(tbpb^{ox2})^{2-}$.

The most salient feature is the characterization of **6**, a dinuclear iron complex, in five different oxidation levels:

(1) The starting complex **6** contains the dianion $[Fe^{III}_2(tbpb)(CN)_4]^{2-}$ with two intramolecularly antiferromagnetically coupled low-spin ferric ions ($S_{Fe} = {}^1/_2$) ($J = -82$ cm^{-1}).

(2) The mixed-valent, one-electron-reduced form $[Fe^{III}Fe^{II}(tbpb)(CN)_4]^{3-}$ contains a low-spin ferric ($S_{Fe} = {}^1/_2$) and a low-spin ferrous ($S_{Fe} = 0$) ion and a diamagnetic bridge $(tbpb)^{4-}$. From the EPR and Mössbauer spectra it can be concluded that this species possesses an $S_t = {}^1/_2$ ground state with localized valencies (class I).

(3) The fully reduced form of **6**, namely the tetraanion $[Fe^{II}_2(tbpb)(CN)_4]^{4-}$, contains two low-spin ferrous ions ($S_{Fe} = 0$) and an overall diamagnetic ground state, $S_t = 0$.

(4) The one-electron-oxidized species of **6**, namely the monoanion $[Fe^{III}_2(tbpb^{ox1\bullet})(CN)_4]^-$, is a three-spin system consisting of two low-spin ferric ions ($S_{Fe} = {}^1/_2$) and a bridging π-radical trianion $(tbpb^{ox1\bullet})^{3-}$. The species possesses

(19) Orbach, R.; Stapleton, H. J. In *Electron Paramagnetic Resonance*; Geschwind, S., Ed.; Plenum Press: New York, London, 1972; pp 121−216.
(20) Pilbrow, J. R. *Transition Ion Electron Paramagnetic Resonance*; Clarendon Press: Oxford, U.K., 1990.

an $S_t = {}^1/_2$ ground state which is shown to result from intramolecular antiferromagnetic interaction between two low-spin ferric ions and a ligand π-radical. The iron−iron exchange coupling constant $J' = -82$ cm^{-1} is found to be the same as in the dianion $[Fe^{III}{}_2(tbpb)(CN)_4]^{2-}$. The iron−radical interaction is also antiferromagnetic and of similar magnitude $J \approx -130$ cm^{-1}.

(5) The fully oxidized species $[Fe^{III}{}_2(tbpb^{ox2})(CN)_4]^0$ contains two antiferromagnetically coupled low-spin ferric ions ($S_{Fe} = {}^1/_2$) yielding the observed diamagnetic ground state.

It is interesting that the mixed-valence species $[Fe^{III}Fe^{II}(tbpb)(CN)_4]^{3-}$ is unstable with respect to disproportionation. The measured comproportionation constant $K_c = 44$ indicates the lack of an electronic stabilization of this form via electron delocalization.

Acknowledgment. The work has been financially supported by the Fonds der Chemischen Industrie.

Supporting Information Available: X-ray crystallographic files in CIF format for complexes **2**−**4** and **6**, tables of X-ray data, and Tables S1 and S2, summarizing infrared spectroscopic data for complexes **1**−**6** and their electronic spectra. This material is available free of charge via the Internet at http://pubs.acs.org.

IC020518Z